

Exceptional points in dielectric spheroid

Evgeny Bulgakov,^{1,2} Konstantin Pichugin,¹ and Almas Sadreev¹

¹*Kirensky Institute of Physics Federal Research Center KSC SB RAS 660036 Krasnoyarsk Russia*

²*Reshetnev Siberian State University of Science and Technology, 660037, Krasnoyarsk, Russia*

(Dated: July 30, 2021)

Evolution of resonant frequencies and resonant modes as dependent on the aspect ratio is considered in a dielectric high index spheroid. Because of rotational symmetry of the spheroid the solutions are separated by the azimuthal index m . By the two-fold variation of a refractive index and the aspect ratio we achieve exceptional points (EPs) at which the resonant frequencies and resonant modes are coalesced in the sectors $m = 0$ for both TE and TM polarizations and $m = 1$.

I. INTRODUCTION

Optical properties of dielectric particle is described by resonant frequencies and corresponding resonant modes. The most famous case is a dielectric sphere whose resonant modes and frequencies were first considered by Stratton [1]. The solutions in the form quasi-normal modes (QNMs) leaking from the sphere were considered in Refs. [2, 3]. The frequencies of these solutions resonances are complex because of coupling of the dielectric particle with the radiation continuum and can be considered as the eigenvalues of the non-Hermitian Hamiltonian [4–7]. Material losses as well as thermal fluctuations [8] of dielectric particle can considerably contribute into the imaginary part of complex resonant frequencies through complex refractive index. Non-Hermitian phenomena drastically alters the behavior of a system compared to its Hermitian counterpart describing the closed system. The best example of such a difference is the avoided resonant crossing (ARC) because of coupling of a particle with the radiation continuum [9–13]. In turn the ARC can emerge to singularities, bound states in the continuum at which the imaginary part of resonance turns to zero [14, 15] that gives rise to collapse of Fano resonance and exceptional points (EPs). The last is remarkable by that complex frequencies become degenerate and the eigenmodes coalesce [16–18]. Early experiments on microwave coupled resonators revealed the peculiar topology of eigenvalue surfaces near exceptional points for encircling of EP [19].

Many works on EPs and their applications are associated with parity-time (PT) symmetric optical systems with a balanced gain and loss. In that case, EPs can be easily found by tuning a single parameter, namely, the amplitude of the balanced gain and loss [20–24]. Since it is not always easy or desirable to keep a balanced gain and loss in an optical system there is of significant interest to explore EPs and their applications in non-PT-symmetric optical systems. Currently, there exist studies concerning EPs for resonant states in extended periodic dielectric structures sandwiched between two homogeneous half-spaces [25–28], dual-mode planar optical waveguides [29] and plasmonic waveguide [30], layered structures [31–33], two infinitely long dielectric cylinders [34–38] and even single rod with deformed cross-section [36, 39–42]. As for compact dielectric resonators we distinguish the only study of EPs in compact coated dielectric sphere [43].

In the present paper we consider similar compact elementary dielectric resonator such as a spheroid in which EPs can be achieved by two-fold variation of aspect ratio and refractive index. Although the spheroid allows the solution due to separation of variables in spheroidal coordinate system [44, 45], analytical expressions for solutions are too cumbersome. We use software package COMSOL Multiphysics which allows to obtain numerically the complex resonant frequencies and corresponding resonant modes of particle of arbitrary shape embedded into the radiation continuum by use of perfectly absorbing boundary conditions.

II. EVOLUTION OF RESONANT FREQUENCIES IN SPHEROID

A rotational symmetry of spheroid implies that the azimuthal index m is preserved. That allows to calculate the resonant frequencies and resonant eigenmodes separately in each sector m and calculate EM field configurations as series over the orbital momenta outside spheroid [44]

$$\vec{E}^{(m)}(\vec{r}) = \sum_{l=1}^{\infty} [a_{lm} \vec{M}_{lm}(\vec{r}) + b_{lm} \vec{N}_{lm}(\vec{r})] \quad (1)$$

where \vec{M}_{lm} and \vec{N}_{lm} are the spherical harmonics [1]. In what follows we consider the sectors $m = 0$ and $m = 1$.

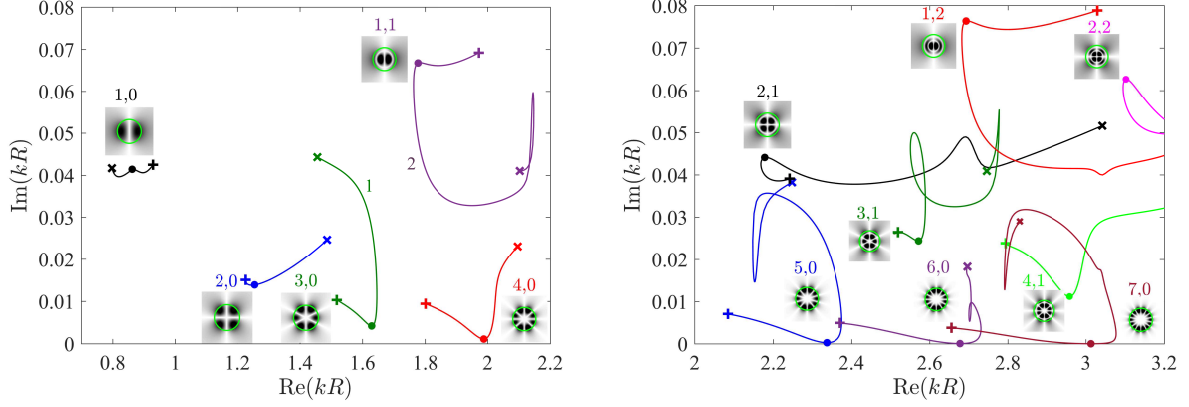


Figure 1. Evolution of complex TE resonant frequencies in silicon spheroid with permittivity $\epsilon = 12$ for variation of aspect ratio of polar R_z and equatorial R_\perp radii in the sector $m = 0$. Wave patterns show azimuthal component of electric field $|E_\phi|$ of the Mie resonant modes in sphere at points marked by closed circles where integers above the insets notify the orbital momentum l and the radial index n . 'x' marks the case of oblate spheroid with $R_z = 0.4R_\perp$ while '+' marks the case of prolate spheroid with $R_z = 1.6R_\perp$.

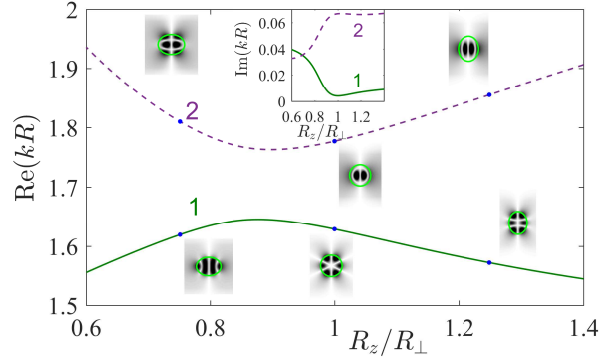


Figure 2. Evolution of resonant frequencies and resonant modes labelled as 1 and 2 in Fig. 1 versus ratio of radii R_z and R_\perp .

The sector $m = 0$ is simplified compared to the sector $m = 1$ because of separation of TE and TM modes. Figure 1 presents evolution of complex TE resonant frequencies with variation of the equatorial radius R_\perp relative to the polar radius R_z from oblate silicon spheroid $R_z = 0.4R_\perp$ to prolate spheroid $R_z = 1.6R_\perp$. k is the wave number, and $R = (R_z R_\perp^2)^{1/3}$ is the mean radius that equalizes volumes of sphere and spheroid. For the reader convenience we split the frequency range in Figure 1 into two parts. The insets show the QNMs of a sphere. In Figure 2 we demonstrate a phenomenon of avoided crossing of resonances marked as 1 and 2 in Figure 1 which is the result of interaction of the dipole QNM with the octuple QNM [46]. There is a general belief that a homogeneous spherical dielectric body represents the ideal case, so that any perturbation of shape of sphere can only degrade the resonance (the imaginary part increases or the Q -factor decreases). Lai *et al* [8, 46] have shown this, however, provided that imaginary part of the spherical QNM is small enough. For the QNMs with low Q -factor their frequencies deviate from the complex eigenfrequencies of sphere linearly [4].

This anomalous behavior of the low- Q resonances can be comprehend if to refer to the series over spherical harmonics (1). For the TE polarization we have

$$E_\phi = \sum_l a_{l0} M_{l0}^\phi \quad (2)$$

where $l = 1, 3, 5, \dots$ if E_ϕ is even relative to $z \rightarrow -z$ and $l = 2, 4, 6, \dots$ if E_ϕ is odd. Once a sphere transforms into spheroid the orbital momentum l is not preserved. Figure ?? shows as new multipole radiation channels are opened with this transformation. Let us consider some of resonances shown Figure 1. For variation of the polar radius R_z the lowest mode shown by black line goes through the Mie dipole mode 1, 0 of a sphere with the frequency

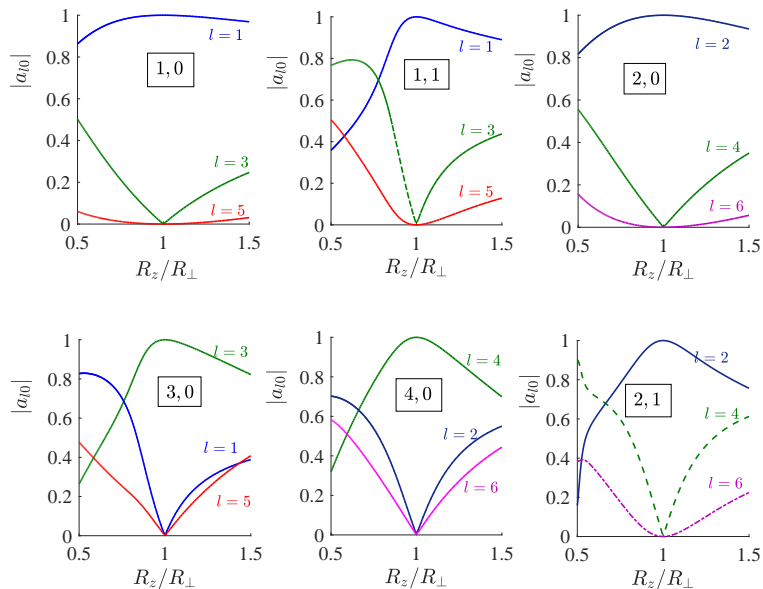


Figure 3. Evolution of multipole coefficients in series (1) for evolution of resonant modes l, n shown in Fig. 1.

$kR = 0.862 + 0.0414i$. As seen from the first subplot of Figure 3 at this moment the only radiation channel is given by the coefficient a_{10} . The resonant widths of the Mie resonant modes fast fall down with the orbital momentum l and grow with the radial index n [47]. As a result, when a sphere is deformed, the fast decaying dipole channel is weakening at the cost of linear arising of the next slower decay octuple channel $l = 3$ in accordance to Eq. (2). These comprehensive considerations were issued by Lai *et al* [46]. Respectively the resonant width is decreased as shown in Figure 1 by black line. However, there are exceptions from this rule, for example, the QNMs $l = 2, n = 1$ and $l = 2, n = 0$ (The last column of subplots in Figure 3). In both cases the same slower decaying radiation channels with $l = 4$ and $l = 6$ are attaching to the quadruple channel with $l = 2$ for deviation from a sphere. Nevertheless the behavior of resonant widths is dramatically different as seen from Figure 1. For the radial quantum $n = 0$ we observe a degradation of the quadruple QNM, while for $n = 1$ we observe the opposite behavior. That shows the importance of the radial indices for resonant widths [47].

Let us consider also the resonances evolving with the Mie resonances with higher orbital momentum, octuple resonance $3, 0$ with the frequency $kR = 1.629 + 0.0042i$ shown by green line in Figure 1. Corresponding evolution of multipole coefficients is shown in Figure 3 in subplot labelled $3, 0$. In contrast to previous dipole and quadruple resonances the high- Q decaying octuple resonance is substituted by the fast decaying dipole resonance $1, 0$. As a result we observe an increase of resonant width in Figure 1 for transformation of sphere into spheroid. Other subplot $4, 0$ in Figure 3 shows the same result.

We omit analysis of the TM resonances shown in Figure 4 because of a similarity with the case of the TE resonances except that the series (1) for magnetic field are given by the coefficients b_{l0} with the same sequence for $l = 1, 3, 5, \dots$ for the even solutions of magnetic field H_ϕ and $l = 2, 4, 6, \dots$ for the odd solutions relative to $z \rightarrow -z$. As a result we have similar rules for resonant widths. The Mie TM dipole and quadrupole resonances yield to spheroid resonances in the Q factor in contrast to the Mie resonances with higher orbital momenta. However there is an exception for the resonance $3, 1$ which have no minimal resonant width at $R_z = R_\perp$. The inset in Figure 4 shows that in the prolate spheroid we have extremely large contribution of the spherical harmonic $l = 5$ compared to the dipole harmonic $l = 1$ that suppresses emission from the prolate spheroid. The sector $m = 1$ is destined to show that the phenomena of ARCs exist in the other sectors of the azimuthal index m , in particular $m = 1$ as demonstrated in Figure 5. Moreover one can observe the same tendency of degradation of the high- Q QNMs and, *visa versa*, enhancement of the Q -factor for the low- Q QNMs for deformation of sphere.

III. EXCEPTIONAL POINTS.

The sector $m = 0$ demonstrates EPs separately for each polarization. Figure 6 shows numerous examples of avoided crossing of TE modes highlighted by open circles. It is interesting that the ARC phenomena are observed only for the oblate spheroids below $R_z/R_\perp = 1/2$. The behavior of QNMs is presented in Figure 7 which shows as the modes

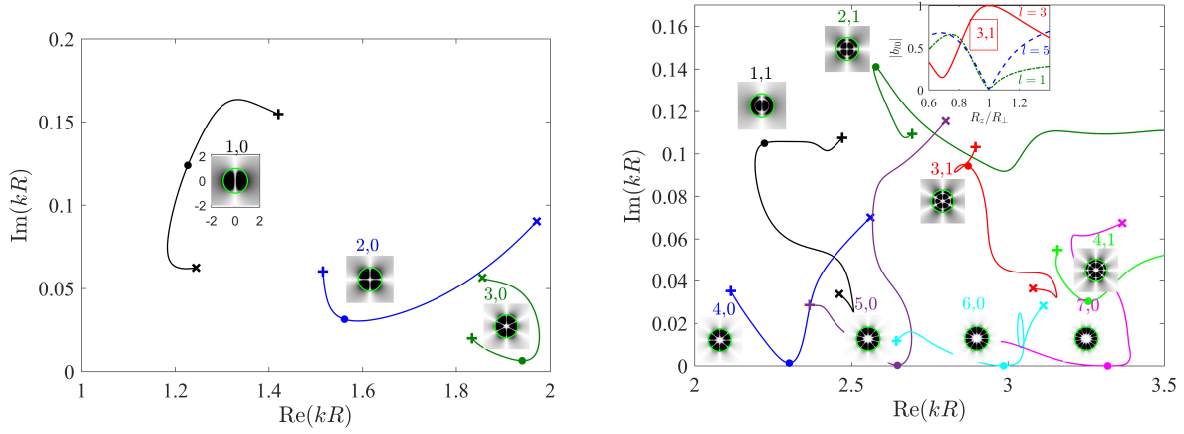


Figure 4. Evolution of complex TM resonant frequencies. Wave patterns show azimuthal component of magnetic field $|H_\phi|$ of the Mie resonant modes. 'x' marks $R_z = 0.4R_\perp$ and '+' marks $R_z = 1.6R_\perp$. The inset shows behavior of multipolar coefficients on the aspect ratio.

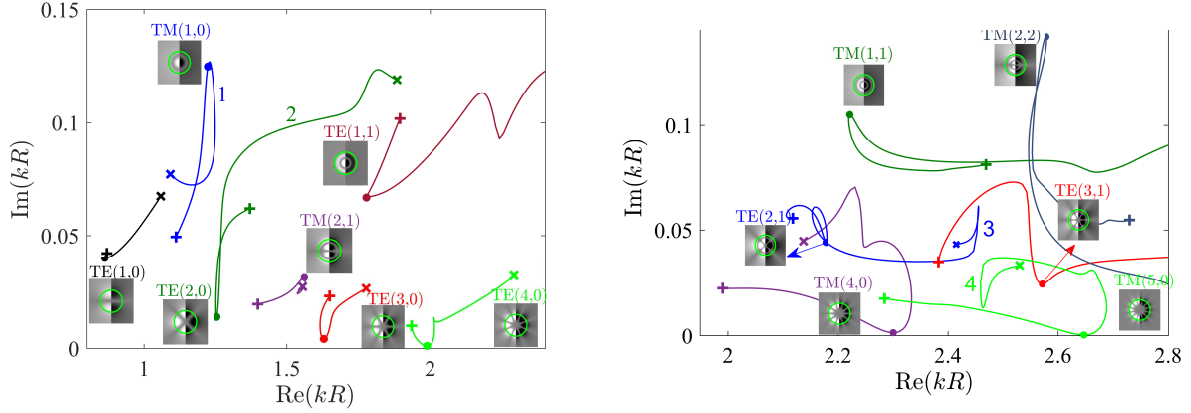


Figure 5. Evolution of resonant frequencies for traversing from the oblate spheroid $R_z = 0.4R_\perp$ (pluses) through a sphere (closed circles) to the prolate spheroid $R_z = 1.6R_\perp$ (crosses) in the sector $m = 1$. Titles above the insets indicate the orbital momentum l and radial index n (the number of radial nodal circles). The TE/TM modes are presented by the azimuthal components $|E_\phi|/|H_\phi|$.

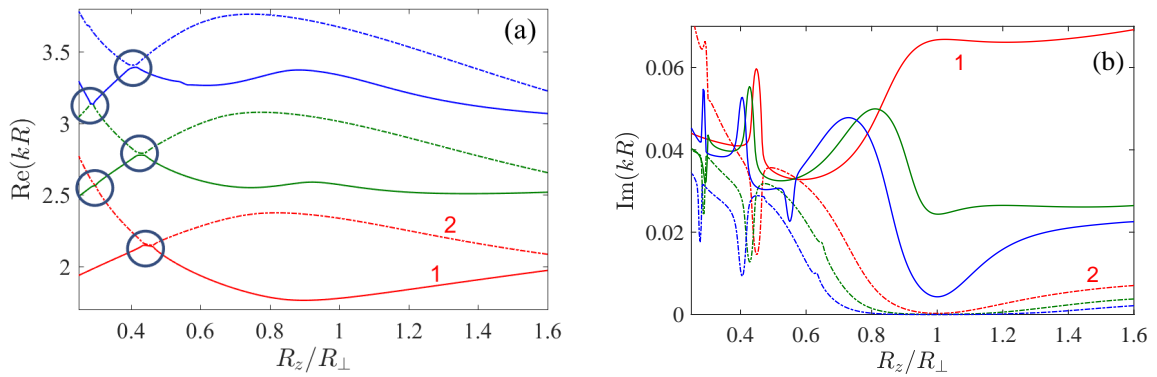


Figure 6. Arcs of TE QNMs for evolution of sphere into spheroid in the sector $m = 0$.

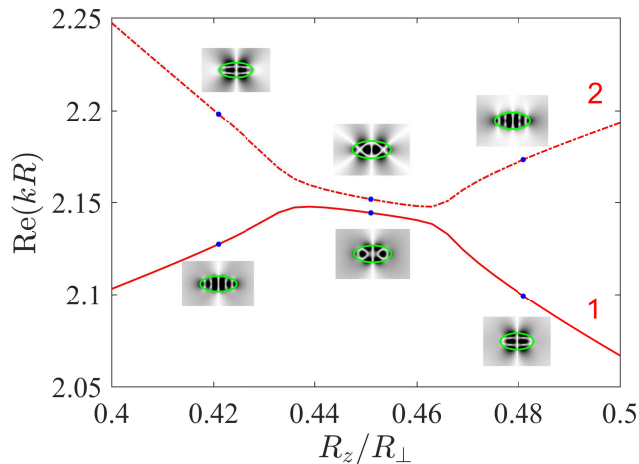


Figure 7. Evolution of selected resonant frequencies and resonant modes labelled as 1 and 2 in Fig. 6 vs ratio of radii R_z and R_\perp . The insets show the azimuthal component $|E_\phi|$ of corresponding resonant modes at points marked by closed circles.

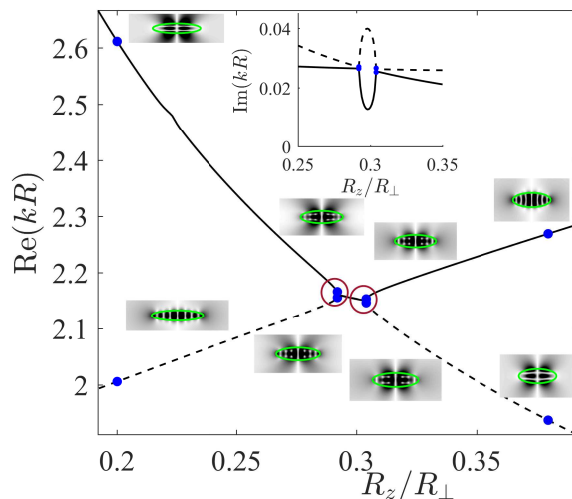


Figure 8. Evolution of resonant frequencies and resonant modes versus R_z/R_\perp at $\epsilon = 17.2$ in the sector $m = 0$. Open circles highlight EPs. The left one at $R_z/R_\perp = 0.292$, $\epsilon = 17.2$ and the right one at $R_z/R_\perp = 0.304$, $\epsilon = 18.4$. The insets show the $|E_\phi|$ profiles of TE QNMs at points marked by closed circles.

are exchanging for variation of the aspect ratio of spheroid. As shown in Figure 6 (b) the ARCs are complemented by strong enhancement of the Q -factor in an agreement with numerous considerations in different dielectric resonators [11, 48–50].

What is remarkable, the oblate spheroid demonstrates numerous EPs for the two-fold variation of the permittivity and the aspect ratio for both sectors $m = 0$ and $m = 1$. Figure ?? shows the behavior of QNMs with the aspect ratio at $\epsilon = 17.2$ in the sector $m = 0$. One can see that inside the areas highlighted by open circles two QNMs coalesce into the one QNM. Such a behavior of resonances close to the EP behavior was observed in different dielectric structures [29, 36, 37, 40, 43]. In order to be convinced that there are indeed the EPs we encircle the EP points shown open circles in Figure ?? by three ways. In the first case the rectangular contour encircles only the left EP at the point $R_z/R_\perp = 0.292$, $\epsilon = 17.2$ as shown in Figure 9 (a). Respectively, in the second case the contour encircles the right EP point $R_z/R_\perp = 0.304$, $\epsilon = 18.4$ as shown in Figure 9 (b). At last, we present also the case of encircling of both EPs shown in Figure 9 (c). In all cases we encircle EPs counterclockwise.

Let us consider the first case shown in Figure 9 (a) where encircling starts with point $R_z/R_\perp = 0.32$, $\epsilon = 17$ marked by open circle in the inset of Figure. In the first downward path we decrease the aspect ratio at the same permittivity reaching the point till $R_z/R_\perp = 0.27$, $\epsilon = 17$ marked by cross. In the complex plane this path maps into sharp

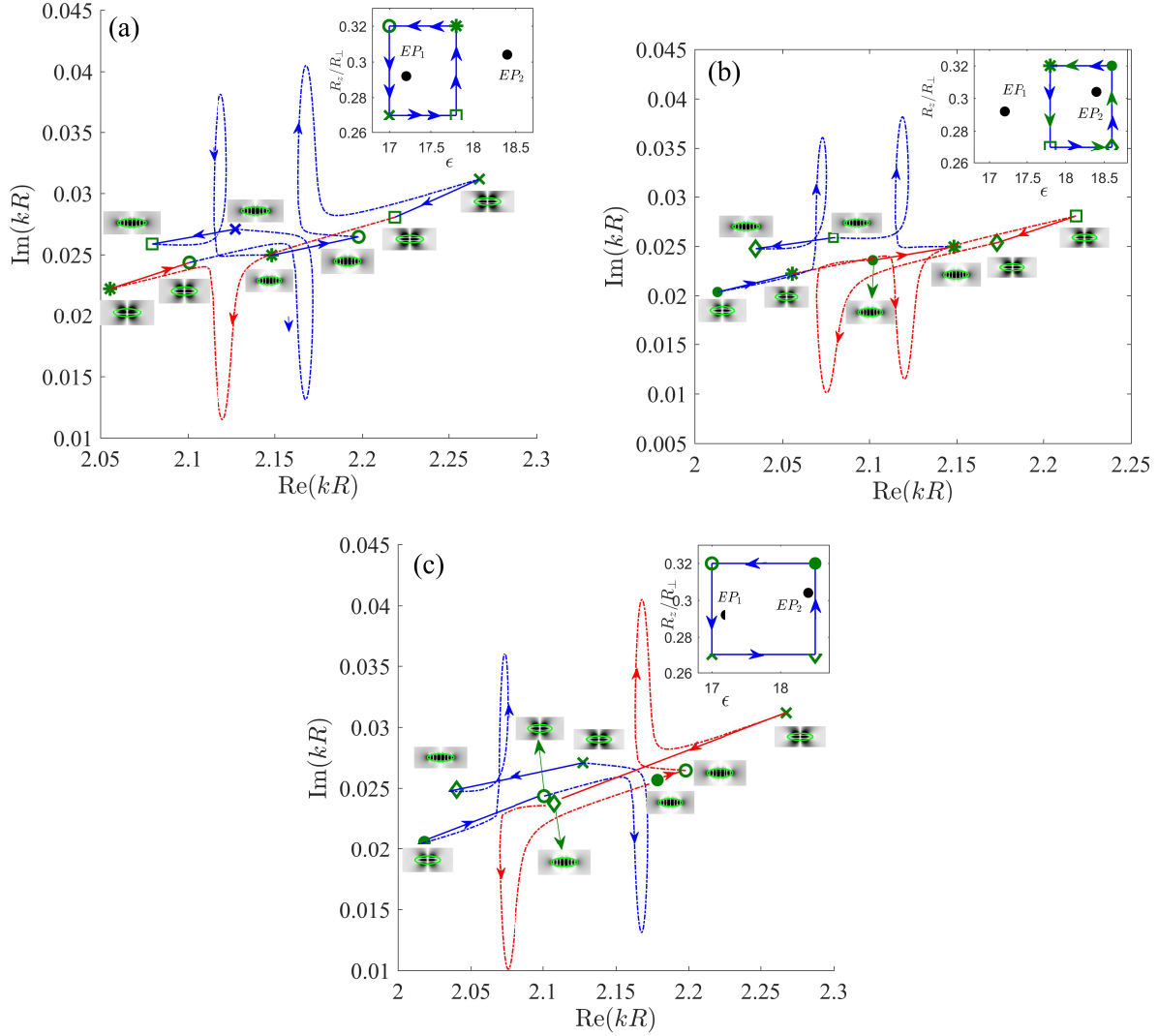


Figure 9. Encircling of EPs shown by open circles in Fig. ?? . (a) and (b) Encircling separate EPs. (c) Encircling of both EPs. Insets show the component E_ϕ of resonant mode.

trajectory shown by dot-dashed blue line that features high response of resonant frequency on shape of spheroid. Respectively the resonant mode demonstrate sharp change of the resonant mode. In the next horizontal path we slightly increase the permittivity from $\epsilon = 17$ till $\epsilon = 17.8$ of the oblate spheroid with the same shape and reach the point $R_z/R_\perp = 0.27, \epsilon = 17.8$ marked by square in the inset. In the complex plane this path maps into monotonic descent of resonant frequency by law $(kR)^2 \epsilon \approx C$ or $kR \approx \sqrt{C/17}(1 - \Delta\epsilon/2)$. That linear part of trajectory is plotted by solid blue line in Figure 9 (a). The resonant mode presented by the insets at starting and finishing points also does not show visible changes. The third upward part of rectangular contour goes from the point marked by square $R_z/R_\perp = 0.27, \epsilon = 17.8$ to the point marked by star $R_z/R_\perp = 0.32, \epsilon = 17.8$ maps into sharp trajectory shown by blue dash line. However the resonant mode is not changing that is related to far distance between the left EP and the path as distinct from the first downward path from circle to cross. By doing so we closed the rectangular contour however as the resonant frequency as the resonant mode are interchanged as was first demonstrated by Dembowskii *et al* in a microwave metallic resonator [19]. And only the second encircling of the left EP restores the resonant mode as demonstrated in Figure 9 (a) by red lines.

The right EP $R_z/R_\perp = 0.304, \epsilon = 18.4$ is expected to give rise to the same features. However as shown in Figure 9 (b) counterclockwise encircling of this EP demonstrates clockwise behavior of the resonant frequency and mode opposite to the case of counterclockwise encircling of the left EP. That is related to that the signs of winding numbers of neighboring EPs arising after crossing of two lines in the complex plane are opposite each other [51, 52]. Figure 9 (c)

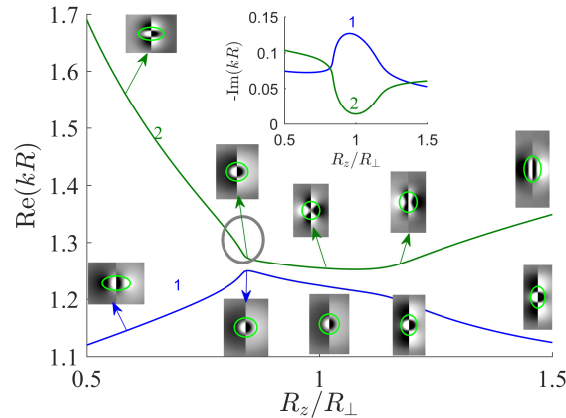


Figure 10. Evolution of resonant frequencies and resonant modes marked as 1 and 2 in Fig. 5 (sector $m = 1$) versus ratio of radii R_z and R_\perp around EPs at $\epsilon = 12$. The EP is given by the point $\epsilon = 12, R_z/R_\perp = 0.84, kR = 1.25$.

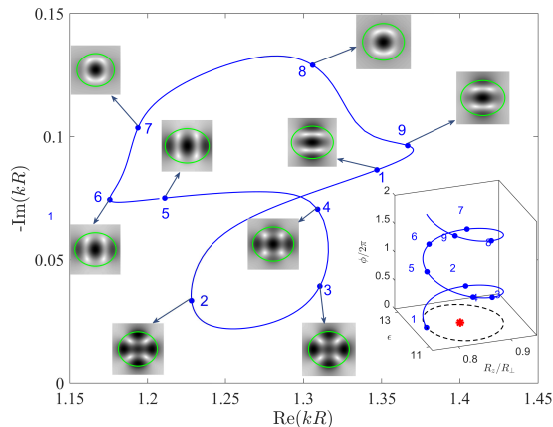


Figure 11. Evolution of the field patterns E_y for encircling the EPs $\epsilon = 12, R_z/R_\perp = 0.84$ marked by star.

presents graphical evidence for that. The one encircling of both EPs restores the resonant modes of each resonance.

Next, we show an existence of EPs in the sector $m = 1$ too in which the QNMs with mixed polarizations can be excited by plane wave incident along the z -axis as different from the case $m = 0$ [1]. The first example of evolution of the QNMs (only the component E_ϕ is presented) and their complex eigenfrequencies in the sector $m = 1$ is presented in Figure 10.

The EPs occur for precise two-fold tuning of the aspect ratio R_z/R_\perp and the refractive index of spheroid that is challengeable experimentally. However there is a way to show EPs by encircling the EP through which resonant eigenmodes are interchanged [19]. Figure 11 demonstrates as for encircling of the EPs in plane R_\perp/R_z and ϵ one of resonant modes restores only after encircling by 4π . It is clear that the same refers to the multipole coefficients a_{l1} and b_{l1} as shown in Figure 3.

There are also many other EPs with higher frequencies. One example of the EP is presented in Figures 13 and 14.

IV. SUMMARY AND CONCLUSIONS

It seems reasonable that resonances of any dielectric particle shaped differently from a sphere yield to the Mie resonances of sphere by the Q -factors because the surface of sphere is minimal. However as Lai *et al* [8, 46] have shown that is truth only for those resonances whose imaginary part is small enough. We present numerous examples which confirm this rule and give comprehensible insight by demonstration of multipole radiation channels for evolution of a sphere into spheroid. However we also show exceptions from this rule.

However the main objective of the present paper was demonstration of EPs in a spheroid that has fundamental

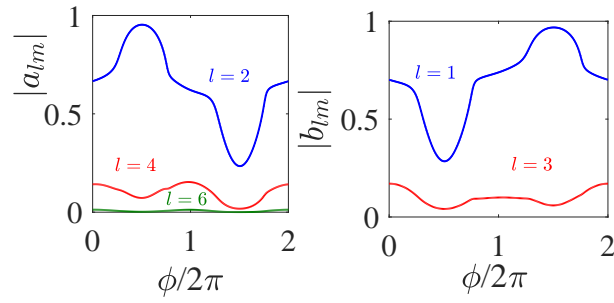


Figure 12. Evolution of the expansion coefficients a_{lm} (TE modes) and b_{lm} (TM modes) for encircling the EP shown in Fig. 11.

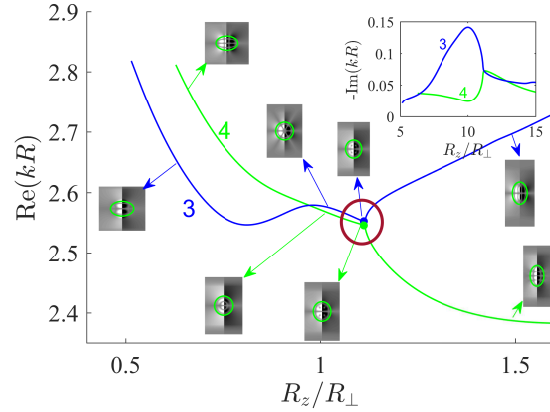


Figure 13. Evolution of resonant frequencies and resonant modes marked as 3 and 4 in Fig. 5 (sector $m = 1$) versus ratio of radii R_z and R_{\perp} around EPs at $\epsilon = 12$. The EP is given by the point $\epsilon = 12.46$, $R_z/R_{\perp} = 1.11$, $kR = 2.56$.

significance because of compactness of these dielectric resonators. Moreover, evolution of expansion coefficients in Fig 6 demonstrate multipole conversion for encircling of EPs and what is the most remarkable this evolution has a period 4π . In the photonic system, the appearance of EPs can be exploited to a broad range of interesting applications, including lasing [53], asymmetric mode switching [29], nonreciprocal light transmission [54, 55], enhancement of the spontaneous emission [56] and ultrasensitive sensing [57].

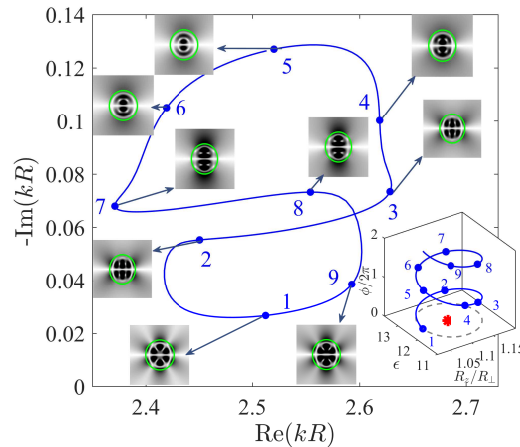


Figure 14. Evolution of the field patterns E_y for encircling the EPs highlighted in Fig. 13.

ACKNOWLEDGMENTS

The work was supported by Russian Foundation for Basic Research projects No. 19-02-00055.

-
- [1] J. A. Stratton, *Electromagnetic theory*, edited by L. A. DuBridge (McGraw-Hill Book Company, Inc., 1941).
- [2] P. Conwell, P. Barber, and C. Rushforth, Resonant spectra of dielectric spheres, *J. Opt. Soc. Am. A* **1**, 62 (1984).
- [3] H. M. Lai, P. T. Leung, K. Young, P. W. Barber, and S. C. Hill, Time-independent perturbation for leaking electromagnetic modes in open systems with application to resonances in microdroplets, *Phys. Rev. A* **41**, 5187 (1990).
- [4] E. S. C. Ching, P. T. Leung, A. M. van den Brink, W. M. Suen, S. S. Tong, and K. Young, Quasinormal-mode expansion for waves in open systems, *Rev. Mod. Phys.* **70**, 1545 (1998).
- [5] P. T. Leung, W. M. Suen, C. P. Sun, and K. Young, Waves in open systems via a biorthogonal basis, *Phys. Rev. E* **57**, 6101 (1998).
- [6] J. Okołowicz, M. Płoszajczak, and I. Rotter, Dynamics of quantum systems embedded in a continuum, *Phys. Rep.* **374**, 271 (2003).
- [7] P. Lalanne, W. Yan, K. Vynck, C. Sauvan, and J.-P. Hugonin, Light interaction with photonic and plasmonic resonances, *Laser & Photonics Reviews* **12**, 1700113 (2018).
- [8] H. M. Lai, P. T. Leung, and K. Young, Limitations on the photon storage lifetime in electromagnetic resonances of highly transparent microdroplets, *Phys. Rev. A* **41**, 5199 (1990).
- [9] W. D. Heiss, Repulsion of resonance states and exceptional points, *Phys. Rev. E* **61**, 929 (2000).
- [10] I. Rotter and A. F. Sadreev, Zeros in single-channel transmission through double quantum dots, *Phys. Rev. E* **71**, 046204 (2005).
- [11] J. Wiersig, Formation of long-lived, scarlike modes near avoided resonance crossings in optical microcavities, *Physical Review Letters* **97**, 10.1103/physrevlett.97.253901 (2006).
- [12] N. R. Bernier, L. D. Tóth, A. K. Feofanov, and T. J. Kippenberg, Level attraction in a microwave optomechanical circuit, *Phys. Rev. A* **98**, 10.1103/physreva.98.023841 (2018).
- [13] K.-W. Park, S. Moon, H. Jeong, J. Kim, and K. Jeong, Non-hermiticity and conservation of orthogonal relation in dielectric microcavity, *J. Physics Communications* **2**, 075007 (2018).
- [14] H. Friedrich and D. Wintgen, Interfering resonances and bound states in the continuum, *Phys. Rev. A* **32**, 3231 (1985).
- [15] A. F. Sadreev, Interference traps waves in an open system: bound states in the continuum, *Rep. Progr. Phys.* **84**, 055901 (2021).
- [16] W. D. Heiss and A. L. Sannino, Avoided level crossing and exceptional points, *J. Phys. A: Math. and Gen.* **23**, 1167 (1990).
- [17] W. Heiss, Phases of wave functions and level repulsion, *The European Physical Journal D - Atom., Mol. and Opt. Phys.* **7**, 1 (1999).
- [18] H. Eleuch and I. Rotter, Width bifurcation and dynamical phase transitions in open quantum systems, *Phys. Rev. E* **87**, 10.1103/physreve.87.052136 (2013).
- [19] C. Dembowski, H.-D. Graf, H. L. Harney, A. Heine, W. D. Heiss, H. Rehfeld, and A. Richter, Experimental observation of the topological structure of exceptional points, *Phys. Rev. Lett.* **86**, 787 (2001).
- [20] M. Brandstetter, M. Liertzer, C. Deutsch, P. Klang, J. Schöberl, H. E. Türeci, G. Strasser, K. Unterrainer, and S. Rotter, Reversing the pump dependence of a laser at an exceptional point, *Nature Communications* **5**, 10.1038/ncomms5034 (2014).
- [21] S. Longhi, Parity-time symmetry meets photonics: A new twist in non-hermitian optics, *EPL (Europhysics Letters)* **120**, 64001 (2017).
- [22] L. Feng, R. El-Ganainy, and L. Ge, Non-hermitian photonics based on parity-time symmetry, *Nature Photonics* **11**, 752 (2017).
- [23] Ş. K. Oezdemir, S. Rotter, F. Nori, and L. Yang, Parity-time symmetry and exceptional points in photonics, *Nature Materials* **18**, 783 (2019).
- [24] M.-A. Miri and A. Alù, Exceptional points in optics and photonics, *Science* **363**, 7709 (2019).
- [25] B. Zhen, C. W. Hsu, Y. Igarashi, L. Lu, I. Kaminer, A. Pick, S.-L. Chua, J. Joannopoulos, and M. Soljačić, Spawning rings of exceptional points out of dirac cones, *Nature* **525**, 354 (2015).
- [26] P. M. Kamiński, A. Taghizadeh, O. Breinbjerg, J. Mørk, and S. Arslanagić, Control of exceptional points in photonic crystal slabs, *Opt. Lett.* **42**, 2866 (2017).
- [27] A. Abdrabou and Y. Y. Lu, Exceptional points of resonant states on a periodic slab, *Phys. Rev. A* **97**, 10.1103/physreva.97.063822 (2018).
- [28] A. Abdrabou and Y. Y. Lu, Exceptional points of bloch eigenmodes on a dielectric slab with a periodic array of cylinders, *Physica Scripta* **95**, 095507 (2020).
- [29] S. N. Ghosh and Y. D. Chong, Exceptional points and asymmetric mode conversion in quasi-guided dual-mode optical waveguides, *Scientific Reports* **6**, 10.1038/srep19837 (2016).
- [30] S. Y. Min, J. Y. Kim, S. Yu, S. G. Menabde, and M. S. Jang, Exceptional points in plasmonic waveguides do not require gain or loss, *Phys. Rev. Applied* **14**, 10.1103/physrevapplied.14.054041 (2020).
- [31] L. Feng, X. Zhu, S. Yang, H. Zhu, P. Zhang, X. Yin, Y. Wang, and X. Zhang, Demonstration of a large-scale optical exceptional point structure, *Optics Express* **22**, 1760 (2013).
- [32] J. Gomis-Bresco, D. Artigas, and L. Torner, Transition from dirac points to exceptional points in anisotropic waveguides,

Phys. Rev. Research **1**, 033010 (2019).

- [33] V. Popov, S. Tretyakov, and A. Novitsky, Brewster effect when approaching exceptional points of degeneracy: Epsilon-near-zero behavior, *Phys. Rev. B* **99**, [10.1103/physrevb.99.045146](https://doi.org/10.1103/physrevb.99.045146) (2019).
- [34] J.-W. Ryu, S.-Y. Lee, and S. W. Kim, Analysis of multiple exceptional points related to three interacting eigenmodes in a non-hermitian hamiltonian, *Phys. Rev. A* **85**, [10.1103/physreva.85.042101](https://doi.org/10.1103/physreva.85.042101) (2012).
- [35] J. Kullig, C.-H. Yi, M. Hentschel, and J. Wiersig, Exceptional points of third-order in a layered optical microdisk cavity, *New Journal of Physics* **20**, 083016 (2018).
- [36] C.-H. Yi, J. Kullig, M. Hentschel, and J. Wiersig, Non-hermitian degeneracies of internal–external mode pairs in dielectric microdisks, *Photonics Research* **7**, 464 (2019).
- [37] Y. Huang, Y. Shen, and G. Veronis, Non-PT-symmetric two-layer cylindrical waveguide for exceptional-point-enhanced optical devices, *Optics Express* **27**, 37494 (2019).
- [38] A. Abdrabou and Y. Y. Lu, Exceptional points for resonant states on parallel circular dielectric cylinders, *J. Opt. Soc. Am. B* **36**, 1659 (2019).
- [39] J. Unterhinninghofen, J. Wiersig, and M. Hentschel, Goos-hänchen shift and localization of optical modes in deformed microcavities, *Phys. Rev. E* **78**, [10.1103/physreve.78.016201](https://doi.org/10.1103/physreve.78.016201) (2008).
- [40] J. Kullig and J. Wiersig, Perturbation theory for asymmetric deformed microdisk cavities, *Phys. Rev. A* **94**, [10.1103/physreva.94.043850](https://doi.org/10.1103/physreva.94.043850) (2016).
- [41] J. Kullig, C.-H. Yi, and J. Wiersig, Exceptional points by coupling of modes with different angular momenta in deformed microdisks: A perturbative analysis, *Phys. Rev. A* **98**, [10.1103/physreva.98.023851](https://doi.org/10.1103/physreva.98.023851) (2018).
- [42] T. Jiang and Y. Xiang, Perturbation model for optical modes in deformed disks, *Phys. Rev. A* **99**, [10.1103/physreva.99.023847](https://doi.org/10.1103/physreva.99.023847) (2019).
- [43] T. Jiang and Y. Xiang, Perfectly-matched-layer method for optical modes in dielectric cavities, *Phys. Rev. A* **102**, [10.1103/physreva.102.053704](https://doi.org/10.1103/physreva.102.053704) (2020).
- [44] S. Asano and G. Yamamoto, Light scattering by a spheroidal particle, *Appl. Opt.* **14**, 29 (1975).
- [45] P. Barber and C. Yeh, Scattering of electromagnetic waves by arbitrarily shaped dielectric bodies, *Appl. Opt.* **14**, 2864 (1975).
- [46] H. M. Lai, C. C. Lam, P. T. Leung, and K. Young, Effect of perturbations on the widths of narrow morphology-dependent resonances in mie scattering, *J. Opt. Soc. Am. B* **8**, 1962 (1991).
- [47] C. C. Lam, P. T. Leung, and K. Young, Explicit asymptotic formulas for the positions, widths, and strengths of resonances in mie scattering, *J. Opt. Soc. Am. B* **9**, 1585 (1992).
- [48] M. V. Rybin, K. L. Koshelev, Z. F. Sadrieva, K. B. Samusev, A. A. Bogdanov, M. F. Limonov, and Y. S. Kivshar, High-Q supercavity modes in subwavelength dielectric resonators, *Phys. Rev. Lett.* **119**, 243901 (2017).
- [49] W. Chen, Y. Chen, and W. Liu, Multipolar conversion induced subwavelength high-q kerker supermodes with unidirectional radiations, *Laser & Photonics Reviews* **13**, 1900067 (2019).
- [50] E. Bulgakov, K. Pichugin, and A. Sadreev, Mie resonance engineering in two disks, *MDPI Photonics* **8**, 49 (2021).
- [51] N. Shvartsman and I. Freund, Vortices in random wave fields: Nearest neighbor anticorrelations, *Phys. Rev. Lett.* **72**, 1008 (1994).
- [52] K.-F. Berggren, A. Sadreev, and A. Starikov, Crossover from regular to irregular behavior in current flow through open billiards, *Phys. Rev. E* **66**, [10.1103/physreve.66.016218](https://doi.org/10.1103/physreve.66.016218) (2002).
- [53] L. Feng, Z. J. Wong, R.-M. Ma, Y. Wang, and X. Zhang, Single-mode laser by parity-time symmetry breaking, *Science* **346**, 972 (2014).
- [54] L. Feng, M. Ayache, J. Huang, Y.-L. Xu, M.-H. Lu, Y.-F. Chen, Y. Fainman, and A. Scherer, Nonreciprocal light propagation in a silicon photonic circuit, *Science* **333**, 729 (2011).
- [55] A. Laha, S. Dey, H. K. Gandhi, A. Biswas, and S. Ghosh, Exceptional point and toward mode-selective optical isolation, *ACS Photonics* **7**, 967 (2020).
- [56] A. Pick, B. Zhen, O. Miller, C. W. Hsu, F. Hernandez, A. Rodriguez, M. Soljačić, and S. Johnson, General theory of spontaneous emission near exceptional points, *Optics Express* **25**, 12325 (2017).
- [57] W. Chen, Özdemir, G. Zhao, J. Wiersig, and L. Yang, Exceptional points enhance sensing in an optical microcavity, *Nature* **548**, 192 (2017).